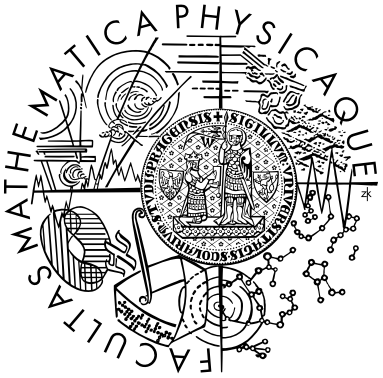

FACULTY
OF MATHEMATICS
AND PHYSICS
Charles University

MASTER THESIS

Václav Alt

Resonant collisions of electrons with diatomic molecules

Institute of Theoretical Physics

Supervisor of the master thesis: RNDr. Karel Houfek, PhD.
Study programme: Physics
Study branch: Theoretical Physics

Prague 2016

I declare that I carried out this master thesis independently, and only with the cited sources, literature and other professional sources.

I understand that my work relates to the rights and obligations under the Act No. 121/2000 Sb., the Copyright Act, as amended, in particular the fact that the Charles University has the right to conclude a license agreement on the use of this work as a school work pursuant to Section 60 subsection 1 of the Copyright Act.

In ..... date ..... signature of the author

Title: Resonant collisions of electrons with diatomic molecules

Author: Václav Alt

Institute: Institute of Theoretical Physics

Supervisor: RNDr. Karel Houfek, PhD., Institute of Theoretical Physics

Abstract: This work aims at calculating the cross sections for vibrational excitation of the oxygen molecules by collisons with electrons. Potential energy curves are obtained with standard quantum chemistry methods and the R-matrix method with good agreement with measurable molecular properties, the cross sections are calculated within the local complex potential approximation. It was shown that the results obtained with different, but seemingly satisfactory settings can vary by a significant degree. Comparison with experimental data then point out the insufficiency of the local complex potential approximation.

Keywords: electron-molecule collisions, potential energy curves, vibrational excitation cross sections, local complex potential approximation, R-matrix method

I would like to thank to my supervisor Karel Houfek for his tireless support, endless patience and enormous amount of consulting. This work could not be finished without all the advice he gave to me.

Contents

Introduction **2**

1 Theoretical methods **3**
1.1 Quantum chemistry calculation methods 3
1.1.1 Wave function construction 3
1.1.2 Hartree-Fock method 4
1.1.3 CI and MCSCF methods 5
1.1.4 Davidson correction 5
1.2 Scattering 6
1.2.1 R-matrix 7
1.3 LCP and cross section 9

2 Potential energy curves **11**
2.1 Quantum chemistry calculations 11
2.1.1 Molpro 11
2.1.2 Symmetry and basis 11
2.1.3 Quantum chemistry calculations 12
2.1.4 Weighted states calculations 13
2.1.5 Spin-orbital splitting 17
2.2 R-matrix calculations 18
2.2.1 R-matrix suite of codes 18
2.2.2 R-matrix models 18

3 The cross sections calculations **21**
3.1 Models comparison 21
3.2 Experiment comparison 22

Conclusion **31**

Bibliography **32**

Introduction

Resonant collisions of electrons with molecules play a significant role in different areas of physics. In applications one usually makes use of the cross sections of various inelastic processes (e.g. vibrational excitations, dissociative attachment or associative detachment). The main goal of this thesis is determination of the cross sections of vibrational excitations of the oxygen molecule O_2. This is done in two main steps, first of which is obtaining potential energy curves and parameters of O_2 and the O_2^- ion, the second is the calculation of the nuclear dynamics and cross sections.

To obtain the potential energy curves, standard *ab initio* quantum chemistry methods are used. This includes the multi-configurational self-consistent field method (MCSCF) and multireference configuration interaction, which are performed using their implementations in the MOLPRO package. Energies of the ion for internuclear distance, at which the additional electron is not bound, are calculated using the R-matrix method, covered with the UKRmol suite of codes. The nuclear dynamics and the cross sections are then handled within the local complex potential approximation.

This approach has already been applied for electron-dioxygen collisions [1, 2], but without any further discussion of the effects of individual models on the results. This work therefore aims at calculating the cross sections with several variations of used settings and comparing them with experimental data.

Unless stated otherwise the atomic units are used in the whole thesis. That means

$$m_e = 1,\ \hbar = 1,\ e = 1,\ \frac{1}{4\pi\varepsilon_0} = 1,$$

where m_e is the mass of an electron, $\hbar$ is the reduced Planck constant, e is the elementary charge and $1/4\pi\varepsilon_0$ is the Coulomb's constant.

1. Theoretical methods

1.1 Quantum chemistry calculation methods

The main goal of quantum chemistry (or molecular quantum mechanics) is to predict properties of molecules in a reliable way. The description of a molecule begins with determining the electronic structure of a molecule, which is usually done by solving the Schrödinger equation, i.e. obtaining the electronic wave function. However the exact solution can only be obtained for the hydrogen atom. To solve for the many-electron wave function, one must therefore reach for approximate methods. This chapter covers several common approximate methods used for solving the many-electron problem, in a brief overview. A more detailed description can be found for example in [3].

Let us consider a system consisting of M nuclei and a total of N electrons. Before writing down the Hamiltonian, we take into account two major approximations:

1. Born-Oppenheimer approximation: the nuclei are considered slow in comparison with the electrons, hence their movement is neglected.

2. At first, all relativistic effects are left aside, but will be partially considered later.

Therefore the Hamiltonian of the system

$$H = -\frac{1}{2}\sum_{i=1}^{N}\nabla_i^2 - \sum_{i=1}^{N}\sum_{j=1}^{M}\frac{Z_j}{\rho_{ij}} + \sum_{i<j}\frac{1}{r_{ij}} + \sum_{i<j}\frac{Z_i Z_j}{R_{ij}}, \tag{1.1}$$

where ρ_{ij} denotes the distance between the i-th electron and the j-th nucleus, r_{ij}, R_{ij} distance between two electrons, nuclei respectively, Z_j is the number of protons in the j-th nucleus. The first term is the kinetic energy of electrons, the second term is electron-proton interaction and the last two terms represent the electronic and protonic repulsion. The problem is now reduced to finding the wave function of N electrons in a fixed potential.

If a system is in a state described by a vector $|\psi\rangle$, i.e. it is the solution of the time-independent Schrödinger equation

$$\hat{H}\,|\psi\rangle = E\,|\psi\rangle\,, \tag{1.2}$$

then the mean energy of the system is given by the expression

$$E = \frac{\langle\psi|\hat{H}|\psi\rangle}{\langle\psi|\psi\rangle}.$$

1.1.1 Wave function construction

The wave function of electrons in a molecule is usually expanded in terms of one electron wave functions called *molecular orbitals*. When accompanied by the spin-part, the term *molecular spin-orbital* is used. Since electrons are fermions, the

wave function must respect the spin statistics, i.e. it has to be fully antisymmetric with respect to an exchange of any two electrons. It is natural to write such a wave function in the form of a Slater determinant, which for a N electron problem looks like this

$$SD(\mathbf{x}_1, \dots \mathbf{x}_N) = \langle x|SD\rangle = \frac{1}{\sqrt{N!}} \begin{vmatrix} \chi_1(\mathbf{x}_1) & \dots & \chi_N(\mathbf{x}_1) \\ \vdots & \ddots & \vdots \\ \chi_1(\mathbf{x}_N) & \dots & \chi_N(\mathbf{x}_N) \end{vmatrix}, \tag{1.3}$$

where $\mathbf{x}_i$ denotes the position of the i-th electron and $1/\sqrt{N!}$ is the normalization factor. Expression $\chi_j(\mathbf{x}_i)$ then means, that the i-th electron occupies the j-th molecular spin-orbital. Of course a linear combination of several Slater determinants can also be taken as the wave function of the system

$$\psi(\mathbf{x}_1, \dots \mathbf{x}_N) = \sum_{i=1}^{K} c_i SD_i(\mathbf{x}_1, \dots \mathbf{x}_N).$$

The following methods are meant to optimize molecular orbitals for the lowest energy.

1.1.2 Hartree-Fock method

In this method every electron is thought to move in an effective field of all the other electrons, which is constructed in a self consisted way, hence the often seen name *self-consistent field method*, or SCF for short. The Hartree-Fock method presumes that the total wave function can be expressed as a single Slater determinant. In such case the mean energy is

$$E = \langle SD|\hat{H}|SD\rangle \,. \tag{1.4}$$

The molecular orbitals minimizing energy (1.4) are found variationally with an additional demand of orthogonality. That leads to the Hartree-Fock equation

$$\hat{F}\,|\chi_i\rangle = \sum_j \varepsilon_{ji}\,|\chi_j\rangle \,, \tag{1.5}$$

where $\hat{F}$ is called the Fock operator and ε_{ji} is a energy matrix. One further assumption is often taken into account, and that is that all the molecular orbitals are considered doubly occupied. The method is then called *restricted Hartree-Fock method* or RHF, otherwise it is *unrestricted Hartree-Fock method* or UHF.

In practice the molecular orbitals are expanded into a certain basis $\{|\phi_i\rangle\}_{i=1}^{K}$ as

$$|\chi_i\rangle = \sum_j c_{ij}\,|\phi_j\rangle \,. \tag{1.6}$$

The Hartree-Fock method thus produces K molecular orbitals, or $2K$ spin orbitals, N of which are occupied by electrons. The remaining $2K - N$ are called *virtual orbitals*.

The assumption of the wave function in the form of a single Slater determinant is however not correct and it does not involve the electron correlation. Because HF is a variational method, it gives only the upper bound for energy:

$$E \leq E_{HF}.$$

The correlation energy is defined as the difference between real and HF energy

$$E_{corr} = E - E_{HF}$$

and is therefore non positive (is zero for one-electron systems).

1.1.3 CI and MCSCF methods

To obtain better results, one may consider using several post-Hartree-Fock methods. One way to obtain correlation energy is to take a linear combination of different Slater determinants as the wave function

$$\Psi_{CI} = d_0(SD_{HF}) + \sum_k d_k^I(SD_k^I) + \sum_{k,l} d_{k,l}^{II}(SD_{k,l}^{II}) + \ldots, \tag{1.7}$$

where d_0, d_k^I, $d_{k,l}^{II}$ are numbers, SD_{HF} is the Hartree-Fock Slater determinant from the previous step and SD_k^I, $SD_{k,l}^{II}$, ... are single, double,... excitations of SD_{HF}. By a single excitation it is meant that one of molecular orbitals in considered Slater determinant is replaced by one of the virtual orbitals. The sum $\sum_k$ in expression (1.7) means, that all possible excitations are made. Double excitation then makes two substitutions in the Slater determinant. Coefficients d_0, d_k^I, $d_{k,l}^{II}$ are then obtained variationally by minimizing the energy. By this approach the mixing (interaction) of different *configurations* (i.e. specific orbital occupations) is considered, therefore this method is called configuration interaction (CI). If all possible excitations are used in (1.7), one usually refers to *full CI* or FCI. The number of possible excitations grows rapidly with the number of electrons and basis size, and FCI quickly becomes computationally demanding. For practical calculations only single and double excitation are typically used (CI-SD).

Another option is the multi-configurational self-consistent field method (MCSCF). It assumes the same form of the wave function but in contrast to CI the molecular orbitals are optimized too. That means that the energy is minimized by varying the coefficients d_0, d_k^I, $d_{k,l}^{II}$ and c_{ij} at the same time. Particularly important special MCSCF method is the *complete active space* SCF method (CASSCF), in which the linear combination (1.7) includes only selected number of orbitals, that span the active space. On this active space FCI and variation of c_{ij} coefficients is performed. CASSCF can be viewed as a combination of CI and HF methods.

Sometimes more then one state is considered for molecular orbitals optimization. *State-averaged* CASSCF (SA-CASSCF) minimizes a weighted average of energies of several chosen states. The advantage of this method is, that the optimized orbitals are also suitable for describing all of the chosen states.

Finally, the multireference configuration interaction (MRCI) uses a combination of *references* or *reference states* (Slater determinants, CASSCF wave functions), from which the excitation are then made.

1.1.4 Davidson correction

A better approximation of the correlation energy can be obtained by considering higher excitations. CI with triple and quadruple excitations (CI-SDTQ) is estimated to give 98 % to 99 % for 20 electron molecules. However CI-SDTQ

method in a basis big enough gets computationally very demanding to be practically useful. But the effect of quadruple excitation on the correlation energy can be approximated by Davidson correction

$$\Delta E_D \approx (1 - d_0)(E_{CI-SD} - E_{HF}), \tag{1.8}$$

where d_0 is the coefficient from expansion (1.7), E_{HF} is energy obtained by a Hartree-Fock method and E_{CI-SD} is the CI-SD energy. That is quite a good approximation of CI-SDTQ energy

$$E_{CI-SDTQ} \approx E_{CI-SD} + \Delta E_D.$$

1.2 Scattering

This section is a brief summary of the description of scattering in [4, 5]. The scattering of an incident electron on a molecule can be schematically written as

$$e^- + M_\alpha \to e^- + M_\beta,$$

where M_α denotes the molecule in an initial state, M_β in final state. Let M be a molecule with N electrons. The scattering is then described with the time-independet Schrödinger equation

$$\hat{H}_{N+1}\psi_E\left(x_1, x_2, \ldots, x_N, x_{N+1}\right) = E\psi_E\left(x_1, x_2, \ldots, x_N, x_{N+1}\right), \tag{1.9}$$

where the energy $E = E_\alpha + E_e$ is the total energy of the system - that means the energy of the molecule in the initial state E_α and the energy of the incident electron E_e. The Hamiltonian can be written in the following form;

$$\hat{H}_{N+1} = \hat{H}_N + \hat{H}_{int}, \tag{1.10}$$

where $\hat{H}_N$ is precisely the previously mentioned Hamiltonian (1.1), while $\hat{H}_{int}$ covers the (N+1)-th electron

$$\hat{H}_{int} = -\frac{\nabla^2_{N+1}}{2} + \sum_{i=1}^{N} \frac{1}{r_{i(N+1)}} - \sum_{i=1}^{M} \frac{Z_i}{\rho_{i(N+1)}}. \tag{1.11}$$

A *scattering channel* is defined as the quantum state of the whole system before or after the collision. It is fully determined by a set of numbers, such as the angular momentum of the projectile electron or the state of the target molecule α. In further discussion, the scattering channels will be denoted simply by lowercase latin letters (i, j,...).

There is an useful ansatz to the form of the wave function, when the electron is far from the molecule, which leads to a natural form of the boundary conditions. The incident electron and the molecule parts are separated:

$$\psi(\mathbf{r}_{N+1}, \xi) = \sum_{i=1}^{n_t} \sum_{j=1}^{n_{c,i}} \Phi_i(\xi)\gamma_{ij}(x_{N+1}). \tag{1.12}$$

The functions $\gamma_{ij}(x_{N+1})$ and $\Phi_i(\xi)$ are the incident electron and target molecule wave functions respectively, $\mathbf{r}_{N+1}$ are the spherical coordinates of the electron and

ξ denotes all relevant degrees of freedom of the target molecule. The sum goes through n_t target states and $n_{c,i}$ channels for target state. Clearly, the function $\Phi_i(\xi)$ obeys the Schrödinger equation

$$\hat{H}_N \Phi_i(\xi) = E_i \Phi_i(\xi)$$

All the observable information about the collision can be retrieved from the wave function $\tilde{\gamma}(r_{N+1})$, which describes the radial behaviour of the scattered electron. The boundary condition then has the form

$$\tilde{\psi}(\mathbf{r}_{N+1}, \xi) \underset{r_{N+1}\to\infty}{\sim} e^{ik_i z}\Phi_i(\xi) + \sum_{j=1}^{n_{ch}} f_{i,j}(\theta,\varphi)\frac{e^{ik_j r_{N+1}}}{r_{N+1}}\Phi_j(\xi), \tag{1.13}$$

where expressions $e^{ik_i z}$, $e^{ik_j r_{N+1}}$ are the incoming plane wave and the outgoing spherical wave with momenta k_i obeying

$$E - E_i = \frac{k_i^2}{2},\ k_i = \sqrt{2(E-E_i)} \tag{1.14}$$

1.2.1 R-matrix

The R-matrix method is an approach to solving the Schrödinger equation for a scattering problem. The main idea of this method lies in separating two parts of the configuration space - the inner and the outer region. In both regions the solution is usually obtained numerically, but in the outer region the calculation is much simpler. The R-matrix is then constructed on the boundary of the two regions (The R-matrix sphere with radius a) and it provides the boundary conditions for the solution of the outer region.

The full scattering wave function ψ_E^Γ is the common eigenfunction of Hamiltonian $\hat{H}_{N+1}$ and operators representing symmetry operations of the irreducible representation Γ of the point group of the molecule. The wave function ψ_E^Γ is expanded in a complete set of states

$$\psi_E^\Gamma(x_1, x_2, \ldots, x_N, x_{N+1}) = \sum_k A_k^E \psi_k^\Gamma(x_1, x_2, \ldots, x_N, x_{N+1}). \tag{1.15}$$

The energy dependence of ψ_E^Γ is supposed to be fully contained only in the coefficients A^E, the energy-independent functions $\{\psi_k^\Gamma\}_k$ are taken as the eigenfunctions of the Hamiltonian

$$\hat{H}' = \hat{H}_{N+1} + \hat{L}, \tag{1.16}$$

where $\hat{L}$ is the *Bloch operator*, which ensures the hermiticity of $\hat{H}'$ in the R-matrix sphere and has the form

$$\hat{L} = \frac{1}{2}\sum_{i=1}^{N+1}\sum_{j=1}^{n_{ch}} |i\rangle\, \delta(r_i - a)\left(\frac{\mathrm{d}}{\mathrm{d}r_i} - \frac{b-1}{r_i}\right)\langle i|\,, \tag{1.17}$$

where a is the R-matrix radius, b is an arbitrary constant and $|i\rangle$ is a state corresponding to the i-th channel. For a more thorough discussion see [4].

The basis functions are called the R-matrix states and can be written in the following form

$$\psi_k^\Gamma(x_1,\ldots,x_{N+1}) = \mathcal{A}\sum_{i=1}^{n_b}\sum_{j=1}^{n_{c,i}}\Phi_i(x_1,\ldots,x_N)\gamma_{ij}(x_{N+1})a_{ijk} + \\ + \sum_{i=1}^{m}\chi_i^\Gamma(x_1,\ldots,x_{N+1})b_{ik}. \quad (1.18)$$

Here the $\Phi_i(x_1,\ldots,x_N)$ are the bound electronic states of the molecule (target) of which n_b are included in the calculation. The functions $\gamma_{ij}(x_{N+1})$ describe the scattered electron, which are the only functions nonzero outside the R-matrix sphere. Finally the functions $\chi_i^\Gamma(x_1,\ldots,x_{N+1})$ are the L^2 integrable functions, zero outside the sphere. The operator $\mathcal{A}$ provides the proper antisymmetrization of the resulting basis function, while functions χ^Γ are assumed to be already antisymmetrized. The superscript Γ indicates, that the wave function tramsforms according to the irreducible representation of the molecule point group. Naturally, only such combinations of functions Φ_i and γ_{ij} that respect the irreducible representation Γ are considered. Note, that a single channel is labeled by two indices, specifying the target and the electron state. Below, the channels will be again denoted by a single index. The total number of channels is $n_{ch} = \sum_{i=1}^{n_b} n_{c,i}$.

Close to the R-matrix radius the function γ_{ij} can be written as

$$\gamma_i(x_{N+1}) \underset{r_{N+1}\to a}{=} \frac{F_i(r_{N+1})}{r_{N+1}}Y_{l_i,m_i}(\Omega_{N+1}), \quad (1.19)$$

where Y_{l_i,m_i} are the spherical harmonics, Ω_{N+1} are the angular variables of $\mathbf{r}_{N+1}$. The R-matrix is defined on the boundary of the inner and outer region, i.e. on the previously mentioned R-matrix sphere. It has the form

$$R_{ij}(E) = \frac{1}{2a}\sum_k \frac{w_{ik}(a)w_{jk}(a)}{E_k - E}, \quad (1.20)$$

where parameter a is the R-matrix sphere radius and $w_{ik} = \langle i|\Psi_k^\Gamma\rangle$ are projections of the scattering channels on the R-matrix states. The meaning of the R-matrix can be seen from the expression

$$F_i(a) = \sum_{j=1}^{n_{ch}} R_{ij}(E)\left(\frac{dF_j}{dr}|_a - bF_j(a)\right),$$

which demostrates, that the R-matrix links the inner and the outer region.

The asymptotical behaviour of the reduced radial wave function $F_i(r)$ is similar to (1.13) - a linear combination of an incoming (R^-) and an outgoing (R^+) solution

$$F_j(r) = \delta_{i,j}R_i^-(r) + K_{i,j}^\Gamma R_j^+(r),\ r\to\infty,$$

where $K_{i,j}^\Gamma$ are the elements of the so-called K-matrix. By diagonalizing the K-matrix one receives an important quantity - the *eigenphase sum*:

$$\delta_{sum}^\Gamma(E) = \sum_{i=1}^{n_{ch}} \arctan[(K_D^\Gamma)_{ii}(E)]. \quad (1.21)$$

In electron-molecule collisions the resonance behaviour is often encountered, which is important for the nuclear dynamics of the process (described in the next section). The presence of a resonance results in a typical dependece of the eigenphase sum on the incident electron energy - a sudden increase by π around the *resonance energy*, which can be described by the Breit-Wigner formula:

$$\delta_{sum}(E) = \delta_r + \delta_{bg} = -\arctan\left(\frac{\Gamma/2}{E - E_r}\right) + \delta_{bg}, \tag{1.22}$$

where the parameters E_r and Γ are the energy (position) and the width of the resonance and δ_{bg} is a non-resonant contribution, typically with only a weak energy dependence.

The calculation is carried out in the so-called "Close-coupling approximation". This means, that in the expansion (1.18) only energetically closely-coupled states are taken into account. A specific closely-coupled R-matrix model is then determined by selecting a number of target and L^2 states. Both of these are usually obtained by a standard CAS (CI) calculation for an N electron problem in the case of Φ_i and $(N+1)$ electrons for L^2 functions χ_i. The structure of these L^2 configurations can be schematically written as

$$\chi_i^{CC} : (core)^{N_c}(CAS)^{N-N_c+1}, \tag{1.23}$$

where $(core)$ represents N_c electrons frozen in doubly occupied target orbitals and (CAS) are the orbitals of the active space. In this kind of model it is also possible to consider occupations of a virtual orbital. In such case the structure is as follows

$$\chi_i^{CC} : (core)^{N_c}(CAS)^{N-N_c}(virtual)^1. \tag{1.24}$$

Sometimes models even allow excitations of the target molecule electrons into the virtual orbitals, which can be a good benefit to the resulting target electronic wavefunction, but it can also be the source of computational trouble.

1.3 LCP and cross section

Local complex potential (LCP) approximation [6] is a simple approach to treating the nuclear dynamics of the negative molecular anion, based on the Born-Oppenheimer approximation. For large internuclear distances, there is typically only one bound electronic state of the molecular anion, that for distances lower than a certain point R_c becomes a resonance state. This point R_c is the crossing point of the potential curves of the neutral molecule and the molecular anion. In practical calculations the resonant part of the potential curve (i.e. the resonance energies) are obtained together with their widths by fitting the eigenphase sum (1.21) with the Breit-Wigner formula (1.22).

The dynamics of the anion state is within the LCP approximation described by the equation

$$\left(E - T_R - V_{res}(R)\right)\xi_E(R) = \zeta_{\nu_i}(R)\chi_{\nu_i}(R), \tag{1.25}$$

$$V_{res}(R) = E_r(R) - \frac{i}{2}\Gamma(R). \tag{1.26}$$

ζ_{ν_i} denotes the *entry amplitude* for capture of the electron in the resonance with the molecule in the initial vibrational state χ_{ν_i}. It is usually taken to be independent of the vibrational state and is determined by the resonance width

$$\zeta_v(R) = \sqrt{\frac{\Gamma(R)}{2\pi}}. \tag{1.27}$$

The resonant vibrational excitation $\nu_i \to \nu_f$ cross section is then given by the expression

$$\sigma^{\mathrm{VE}}_{v_\mathrm{i}\to v_\mathrm{f}}(E) = \frac{4\pi^3}{k^2_\mathrm{ei}} \left| \int_0^\infty dR\, \chi_{v_\mathrm{f}}(R)\zeta_{v_\mathrm{f}}(R)\xi_E(R) \right|^2, \tag{1.28}$$

with ζ_{v_f} being the *exit amplitude* which is again given by (1.27).

2. Potential energy curves

This section describes the calculation of the potential energy curves of O_2 and its ion. For reasons outlined in the theoretical section, the calculation is divided into two steps:

1. the potential curve of O_2 and the bound part of O_2^- curve are obtained via the quantum chemistry methods,

2. the resonant part of O_2^- curve is then obtained with the R-matrix method.

2.1 Quantum chemistry calculations

2.1.1 Molpro

All the following calculations are performed using the quantum chemistry package MOLPRO [7, 8], which is a system of *ab initio* programs used in molecular electonic structure calculations. The Hartree-Fock method (HF), multi-configurational self-consistent field method (MCSCF) and multireference configuration interaction (MRCI), described above in the theoretical section, are implemented as programs HF, MULTI [9, 10] and MRCI [11] respectively.

2.1.2 Symmetry and basis

The molecular spin-orbitals used to construct the molecular electronic wave function are usually obtained by the LCAO method, i.e. taking a linear combination of atomic orbitals (AOs) located on individual atoms. For the sake of numerical calculations a finite set of basis functions must be taken. Hydrogen-like (sometimes Slater type orbitals or STOs) atomic orbitals (i.e. $\propto exp(-\xi r)$) are not a good choice, because their integrals (in matrix elements etc.) are difficult to evaluate. Because of that, so called Gaussian type orbitals or GTOs ($\propto exp(-\xi r^2)$) are usually taken instead. To approximate STOs, linear combinations of GTOs for a few different values of parameter ξ are made. In the context of MOLPRO calculations basis elements (GTOs) are called primitive AOs, their linear combinations (≈STOs) are called contractions.

Once the symmetry point group of the moecule is identified, linear combinations of basis functions, which transform according to individual irreducible representations are made. These symmetry adapted linear combinations (SALCs) form a new basis, which is then used to construct the molecular orbitals. Such basis brings a great advantage - thanks to the Wigner-Eckart theorem, only linear combinations of basis functions of one irreducible representation are relevant, because matrix elements between states transforming according to different irreducible representations are identically zero.

Symmetry operations of the oxygen molecule form the $D_{\infty h}$ point group, but that one is not implemented in MOLPRO . Instead, the largest available subgroup $D_{2h} \subset D_\infty$ is used. Irreducible representations of $D_{\infty h}$ are generally reducible in D_{2h} group and therefore their reduction in terms of D_{2h} irreducible representations has to be used.

In upcoming calculations the ground state of O_2 ($X^3\Sigma_g^-$) and four lowest terms of O_2^- ($^2\Pi_g$, $^4\Sigma_u^-$, $^2\Sigma_u^-$, $^2\Pi_u$) are included. The $D_{\infty h}$ representations assigned to these terms and their corresponding D_{2h} reductions are in Table 2.1. The important thing is that the representations of the states $^2\Pi_g$ and $^2\Pi_u$ are both doubly degenerate in the D_{2h} point group, which leads to a total of six O_2^- states included in potential curves calculations.

$D_{\infty h}$	D_{2h}	conf.
$X^3\Sigma_g^-$	$^3B_{1g}$	$[core]1\pi_u^4 1\pi_g^2$
$^2\Pi_g$	$^2B_{2g} + {}^2B_{3g}$	$[core]1\pi_u^4 1\pi_g^3$
$^4\Sigma_u^-$	^4A_u	$[core]1\pi_u^4 1\pi_g^2 3\sigma_u$
$^2\Sigma_u^-$	^2A_u	$[core]1\pi_u^4 1\pi_g^2 3\sigma_u$
$^2\Pi_u$	$^2B_{2u} + {}^2B_{3u}$	$[core]1\pi_u^3 1\pi_g^4$

Table 2.1: The lowest O_2 and four lowest O_2^- state term symbols and their molecular electron configurations; $[core] = 1\sigma_g^2 1\sigma_u^2 2\sigma_g^2 2\sigma_u^2 3\sigma_g^2$

2.1.3 Quantum chemistry calculations

The aim of this part is to calculate potential curves for O_2 molecule and O_2^- ion. One way to make sure that the resulting curves are relevant to reality is to check for the electron affinity (EA) of O and O_2 or the dissociation energy (DE), because these were already determined by experiment. The EA(O) is defined as the amount of energy released when an electron is added to the atom, i.e.

$$\mathrm{O} + e^- \rightarrow \mathrm{O}^- + \mathrm{EA(O)}.$$

The $EA(O_2)$ has the same meaning, but for the molecule:

$$\mathrm{O_2} + e^- \rightarrow \mathrm{O_2^-} + \mathrm{EA(O_2)}.$$

The dissociation energy is the amount of energy that needs to be added to the molecule to dissociate

$$\mathrm{O_2} + \mathrm{DE(O_2)} \rightarrow 2\mathrm{O}.$$

The O_2 molecule is thought to be in the lowest vibrational state, therefore DE is the difference between the asymptotic energy of the potential curve and the lowest vibrational level, not the bottom of the potential well.

The desired values of these energies are [12]:

$\mathrm{EA(O)} = 1.4611096 \pm 0.0000007$ eV,

$\mathrm{EA(O_2)} = 0.450 \pm 0.002$ eV,

$\mathrm{DE(O_2)} = 5.165 \pm 0.002$ eV.

All calculations had a common structure

1. Hartree-Fock for one fixed geometry to get an initial guess for molecular orbitals,

2. CASSCF for a range of internuclear distances to optimize the molecular orbitals,

3. MRCI for the same geometries as CASSCF to get a better variational energy.

When starting a new calculation, MOLPRO uses the results of previous calculations, hence the first Hartree-Fock calculation is done only to get some rough idea of the molecular orbitals. The purpose of CASSCF is to estabilish suitable molecular orbitals and the MRCI then improves the energy. Throughout all quantum chemistry calculations the bases cc-pVXZ and aug-cc-pVXZ were used [13, 14].

To reduce the computational cost some orbitals were kept *closed*, that means that excitations from these orbitals were forbidden in the whole calculation. In MOLPRO the closed orbitals and CAS are specified by choosing the number of orbitals for each irreducible representation. In all CASSCF calculations the core orbitals $1\sigma_g^2 1\sigma_u^2$ with 4 electrons were kept closed, but the CAS varied.

2.1.4 Weighted states calculations

Although this work covers only low energy electron-molecule collisions (i.e. within 2.5 eV range), for future calculations with higher energies, the molecular orbitals were optimized with respect to four lowest O_2^- states: $^2\Pi_g$, $^4\Sigma_u^-$, $^2\Sigma_u^-$, and $^2\Pi_u$. Note, that since the representations of $^2\Pi_g$ and $^2\Pi_u$ are both doubly degenerate in the D_{2h} point group, one comes to the total of six O_2^- states. The molecular orbitals were therefore optimized using the SA-CASSCF method.

Without further specification, MOLPRO treats all considered state energies equally, i.e. with the same weight, while optimizing the molecular orbitals. This however resulted in an unwanted bump on the $^2\Pi_g$ curve, as can be seen in Figure 2.1, top panel. The reason behind this bump is probably that the CASSCF calculation is not reliable for internuclear distances, where the $(N+1)$-th electron bound state becomes a resonance.

To eliminate the rise of $^2\Pi_g$ energy, the weights of the states were set to change dynamically with internuclear distance. For shorter internuclear distances only the $^2\Pi_g$ state is taken into account with weight 0.5 (because it is degenerate in D_{2h} point group), for greater distances all states were weighted equally with 1/6. Inbetween the weights changed smoothly according to a 3rd degree polynomial shown in Figure 2.2. This eliminated the bump succesfully, see Figure 2.1, bottom panel.

Another option to eliminate the bump would be optimizing the molecular orbitals with respect to the $^2\Pi_g$ only, but this resulted in rather bad affinities and was therefore discarded.

Figure 2.1 still shows bad behaviour of $^2\Sigma_u^-$ state for internuclear distance around 5 *a.u.* and MRCI calculations for $^4\Sigma_u^-$ tend to fail. Since this work's objective is to cover only the lower energy colisions, the higher states of O_2^-, namely $^4\Sigma_u^-$, $^2\Sigma_u^-$, and $^2\Pi_u$ (degenerate), are from this point involved only in the CASSCF calculation to obtain relevant molecular orbitals, and the MRCI is preformed only for the $X^3\Sigma_g^-$ and $^2\Pi_g$ states.

Because for scattering calculations the absolute position of O_2 and O_2^- potential curves is irrelevant and only their correct relative position is important, a

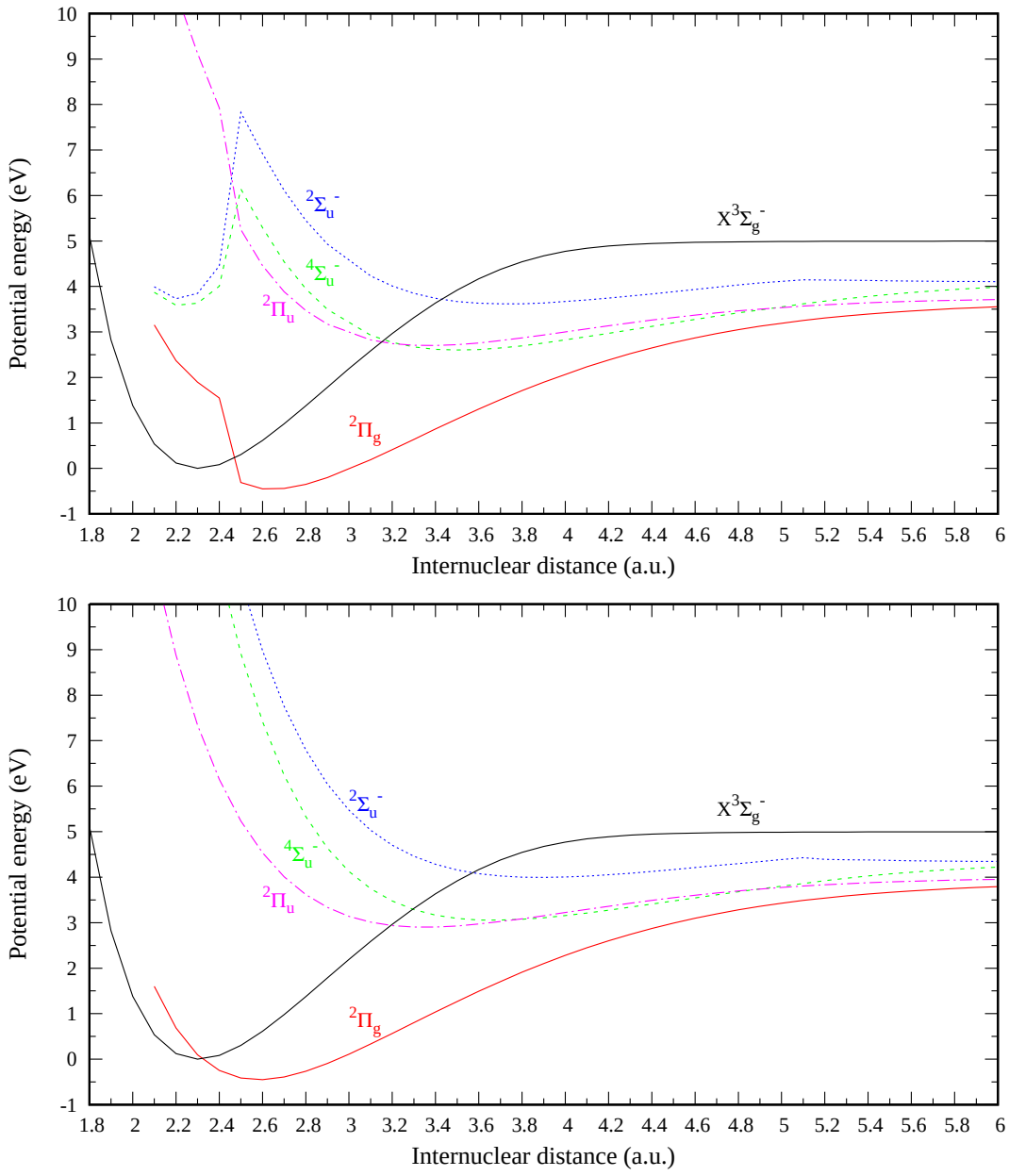

Figure 2.1: SA-CASSCF energies of lowest O_2^- states with CASSCF energy of $X^3\Sigma_g^-$. Top panel: all six states treated with equal weigths; Bottom panel: calculation with dynamically changing weights; The $X^3\Sigma_g^-$ is shown only for better illustration. Its precise position is not consistent with O_2^- curves of SA-CASSCF calculation.

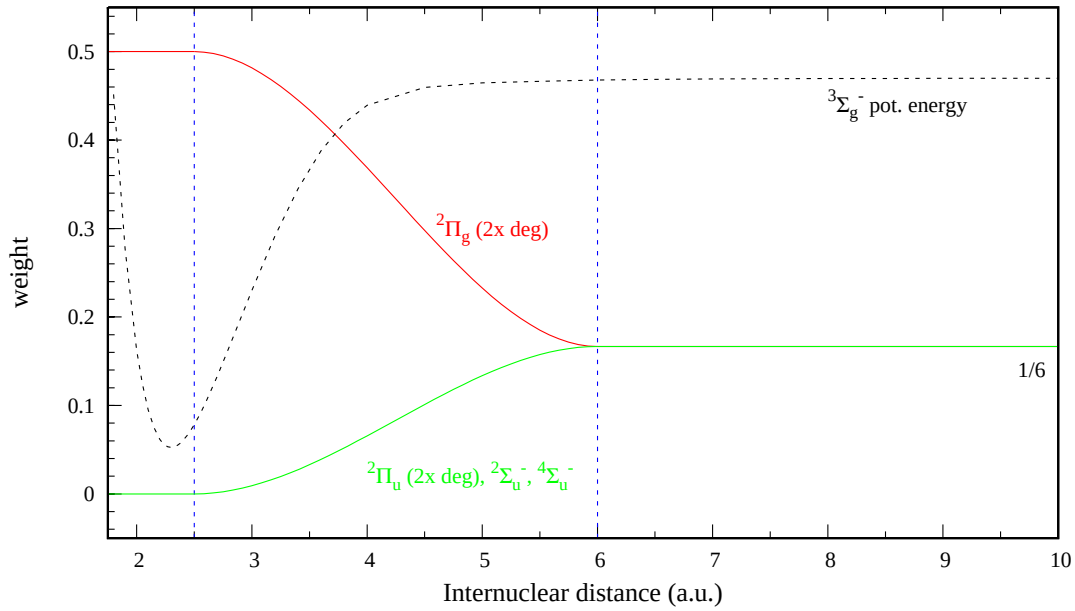

Figure 2.2: Dynamic weight distribution, $^3\Sigma_g^-$ potential energy curve is shown for better illustration

better agreement of the EAs with experimental values can be achieved by shifting the O_2^- potential. If the calculations of potential curves are consistent and their shape is in good agreement with reality, the EAs should agree.

To calculate EA(O_2) energies of vibrational levels in the potential curves were needed. These were calculated with program [15], which is later in this work used also for the cross sections calculations.

Series of calculations with different CAS settings in different bases and with and without Davidson correction (DC) were carried out in order to find a setting with the best affinities. Results for the aug-cc-pVQZ basis are listed in Table 2.2. Two values of EA(O_2^-) are missing, because the calculation of the vibrational levels failed for unresolved reasons. The best results were obtained with CAS= $\{2\sigma_g 2\sigma_u 3\sigma_g 1\pi_u 1\pi_g 3\sigma_u 2\pi_u 2\pi_g\}$ in bases aug-cc-pVXZ, slightly improving with growing bases (i.e. increasing X), as can be seen in Table 2.3. The largest base available is aug-cc-pV6Z, however the resulting energies can be extrapolated in terms of basis size (in detail in [16]):

$$E_n = \frac{(n-1)^3 E_{n-1} - (n-2)^3 E_{n-2}}{(n-1)^3 - (n-2)^3}, \tag{2.1}$$

where n denotes the basis (e.g. $n = 4$ denotes the aug-cc-pVQZ basis).

Two curves with the best results are listed in Table 2.4. The extrapolated curve in aug-cc-pV7Z with DC was then deformed to match the experimental affinities and taken as a third curve. All three curves can be seen in Figure 2.3. At first sight they seem very close to each other, but further calculations show that these differences are crucial.

CAS	$(\ldots)2\pi_u2\pi_g$	$(\ldots)4\sigma_g2\pi_g$	$(\ldots)4\sigma_g2\pi_u2\pi_g$	$(\ldots)4\sigma_g2\pi_u5\sigma_g$	DC
$EA(O_2)$	0.776	0.366	×	0.372	×
EA(O)	1.264	0.971	1.045	1.019	×
$EA(O_2)$	0.963	0.856	×	0.814	×
EA(O)	1.461	1.461	1.461	1.461	×
$EA(O_2)$	0.412	0.330	0.331	0.336	✓
EA(O)	1.380	1.232	1.287	1.268	✓
$EA(O_2)$	0.493	0.559	0.505	0.529	✓
EA(O)	1.461	1.461	1.461	1.461	✓

Table 2.2: Electron affinities of O and O_2 for different CAS settings in aug-cc-pVQZ basis. All affinities are in eV, highlighted rows display affinities after $^2\Pi_g$ curve was shifted so that EA(O) agreed with the experimental value 1.461 eV. $(\ldots) = 2\sigma_g2\sigma_u3\sigma_g1\pi_u1\pi_g3\sigma_u$, DC - Davidson correction.

aug-cc-pV	QZ	5Z	6Z	7Z	DC
$EA(O_2)$	0.442	0.460	0.470	0.484	×
EA(O)	1.241	1.258	1.268	1.280	×
$EA(O_2)$	0.663	0.663	0.663	0.664	×
EA(O)	1.461	1.461	1.461	1.461	×
$EA(O_2)$	0.412	0.427	0.434	0.444	✓
EA(O)	1.357	1.376	1.385	1.398	✓
$EA(O_2)$	0.516	0.512	0.510	0.507	✓
EA(O)	1.461	1.461	1.461	1.461	✓

Table 2.3: Electron affinities of O and O_2 for CAS = $\{2\sigma_g2\sigma_u3\sigma_g1\pi_u1\pi_g3\sigma_u$ $2\pi_u2\pi_g\}$ for bases aug-cc-pV(QZ-6Z) and extrapolated to aug-cc-pV7Z. All affinities are in eV, highlighted rows display affinities after $^2\Pi_g$ curve was shifted so that EA(O) agreed with experimental value 1.461 eV, DC - Davidson correction.

curve	basis	DC	EA(O)	$EA(O_2)$	$EA_{shift}(O_2)$	$DE(O_2)$
I	aug-cc-pV6Z	×	1.268	0.470	0.662	5.101
II	aug-cc-pV7Z	✓	1.398	0.444	0.506	5.161
III	aug-cc-pV7Z def.	✓	1.461	0.450	×	5.162

Table 2.4: MOLPRO results, $EA_{shift}(O_2)$ denotes the electronic affinity of O_2 after the EA(O) has been shifted to its experimental value of 1.461 eV, DC - Davidson correction.

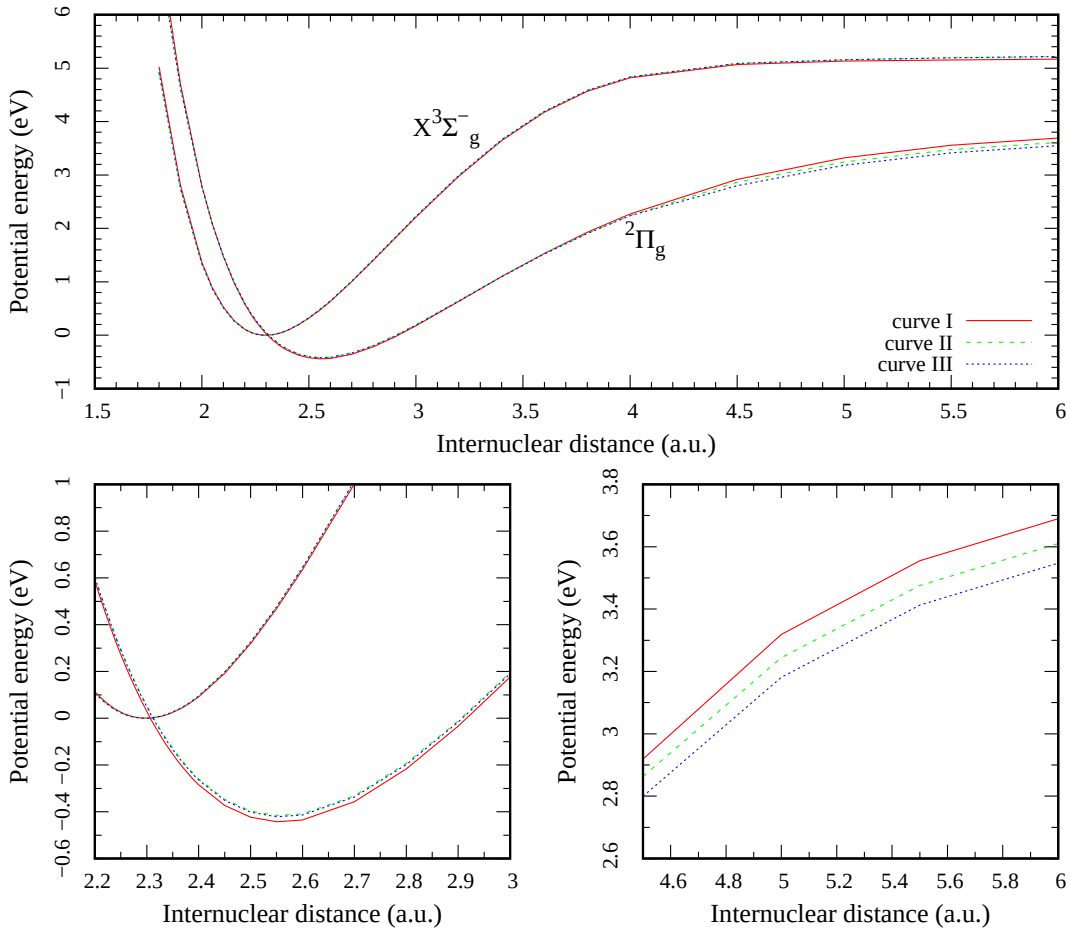

Figure 2.3: Resulting MOLPRO curves, as listed in Table 2.4

2.1.5 Spin-orbital splitting

For the final comparisson with the experimental data, it was necessary to compute the spin-orbital (SO) splitting of the $^2\Pi_g$ state. The spin-orbital splitting calculation was done by diagonalizing the spin-orbital matrix using MOLPRO's implementation within the MRCI program, using a smaller basis [17] cc-pVTZ basis (comparison with experimental data shows that this is sufficient). The splitting magnitude, i.e. the energy difference between these split states, is in Figure 2.4. To obtain SO splitting values for all needed geometries a Gaussian fit was performed,

$$f(x) = a\exp(-b(x-c)^2) + d,$$

with resulting values $a = 6.985$, $b = 0.1253$, $c = 2.460$, $d = 12.266$.

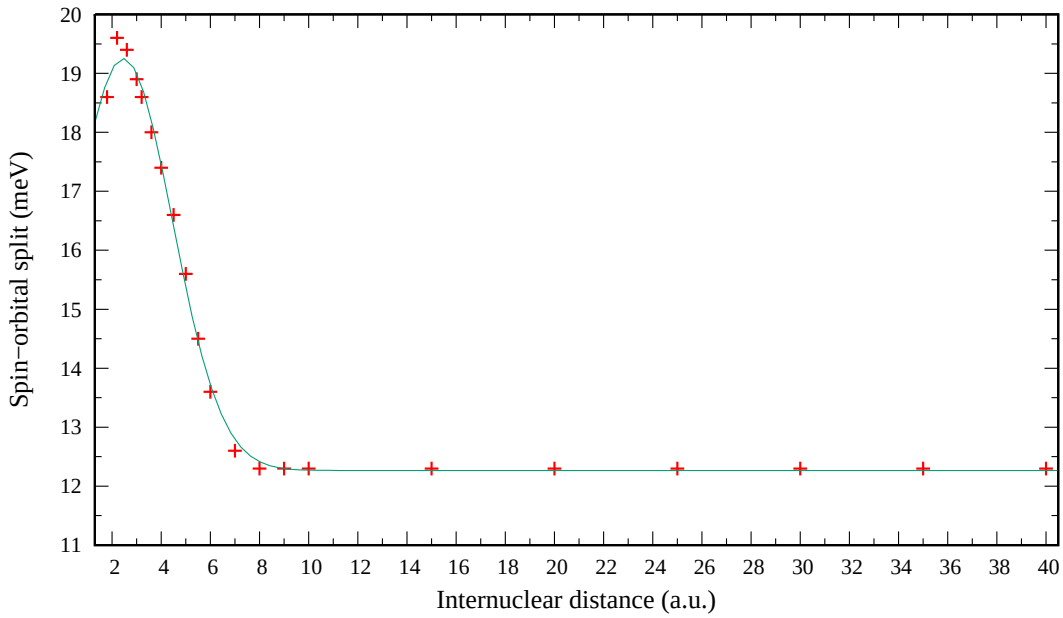

Figure 2.4: Magnitude of the spin-orbital splitting of $^2\Pi_g$ state dependence on internuclear distance with a Gaussian fit

2.2 R-matrix calculations

2.2.1 R-matrix suite of codes

For all the R-matrix calculations in this thesis the UKRmol suite of codes [18] was used. The structure of the calculations within this implementation looks like this

1. Target calculation
2. Inner region calculation
3. Outer region calculation

In the first step the Φ_i functions of the molecule are produced through Molpro's implementation of CASSCF. The model is set by choosing frozen, CAS and virtual orbitals, which is done, as in the case of Molpro, by marking number of states of each irreducible representation of the symmetry point group. In the inner region calculations coefficients a_{ijk}, b_{ik} are obtained by diagonalizing the Hamiltonian. In the last step the R-matrix is constructed, the K-matrix and the eigenphase sums are obtained.

2.2.2 R-matrix models

The molecular orbitals were optimised with respect to the energy of the O_2 ground state $^3\Sigma_g^-$ in cc-pVTZ basis. At present, it is practically impossible to use a larger basis since scattering calculations are computationally too demanding. The core and active space remained unchanged throughout all the calculations:

$(core) = 1\sigma_g 1\sigma_u$

$(CAS) = 2\sigma_g 2\sigma_u 3\sigma_g 1\pi_u 1\pi_g 3\sigma_u$

The model was then varied only by choosing different subsets of possible target states and different number of virtual states. From all possible target states of O_2, only those lying energetically under the $O(P) + O(P)$ asymptote were considered, namely $X^3\Sigma_g^-$, $^1\Delta_g$, $^1\Sigma_g^+$, $^1\Sigma_u^-$, $^3\Delta_u$ and $^3\Sigma_u^+$. Since the Δ irreducible representations are doubly degenerate in the D_{2h} point group, it leads to the maximum of 8 possible target states. Each R-matrix model will therefore be denoted by the number of target and virtual states. In all R-matrix calculations the R-matrix sphere radius was set to 10 a_0, which is sufficient for R-matrix calculations with short internuclear distances.

Let us introduce a shorthand notation for the R-matrix models: an R-matrix model with k virtual orbitals and l target states will be denoted as kv, lt R-matrix model, or just kv, lt model. For example MOLPRO *curve I and the R-matrix model with 8 virtual orbitals and 5 target states* becomes MOLPRO *curve I with* $8v, 5t$ *R-matrix model*.

With quantum chemistry methods the potential curves of O_2 and O_2^- are obtained, but for internuclear distances lower than the crossing point of the $X^3\Sigma_g^-$ and $^2\Pi_g$ curves the calculation of the $^2\Pi_g$ is not reliable and does not provide any information about the resonance width. This resonant part is obtained from the R-matrix calculation since it produces the $(N+1)$-electron wave function, the energy of which is exactly the energy of $^2\Pi_g$ state of O_2^-. An R-matrix model for which the potential energy curve of $^2\Pi_g$ was a smooth continuation of MOLPRO curve in the lower internuclear distance would be an ideal one. To find the best R-matrix model the resulting potential energy curves for $X^3\Sigma_g^-$ state obtained by MOLPRO and R-matrix method were shifted to overlap and the R-matrix models resulting in best continuation of $^2\Pi_g$ curve were chosen. The effect of changing the number of virtual orbitals or target states on the resulting R-matrix energy is illustrated in Figure 2.5. Selected satisfactory models for the three curves chosen in the previous section are listed in Table 2.5. Note, that there is one R-matrix model that suited acceptably for all three MOLPRO curves.

The spin-orbital split was considered in two ways:

1. The R-matrix model was found for the unsplit curve and the SO split was then performed on the resulting R-matrix+MOLPRO curve.

2. The MOLPRO curve was split and for each curve R-matrix model was found. However the split is very small and each curve ended up with the same R-matrix model.

The first approach is inconsistent, because the split curves are then accompanied by the same resonance widths while they should be different. The cross section calculations however revealed negligible difference between these two approaches. All following results were obtained through the second approach.

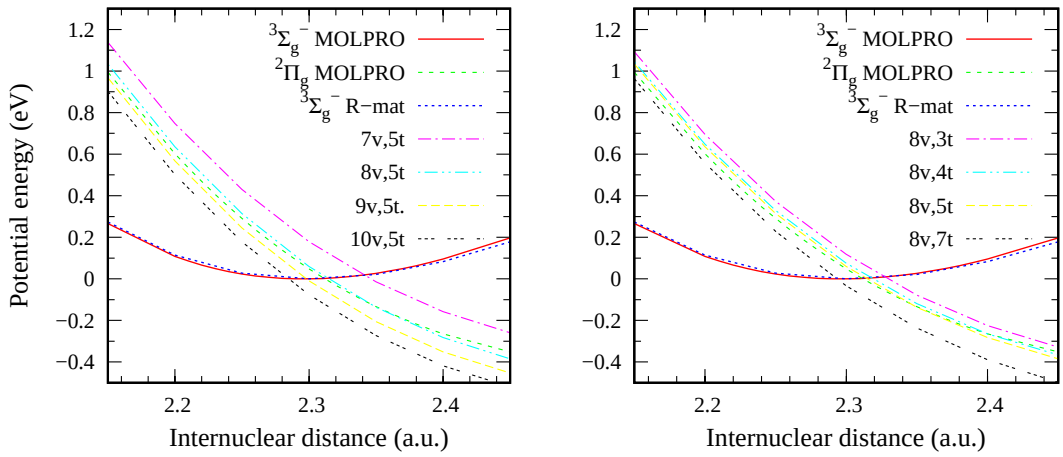

Figure 2.5: MOLPRO curve III with potential energy curves for various numbers of virtual and target states.

curve	R-mat. model
I	8 virtual orb., 5 target st.
	9 virtual orb., 3 target st.
	9 virtual orb., 4 target st.
II	7 virtual orb., 8 target st.
	8 virtual orb., 4 target st.
	9 virtual orb., 3 target st.
III	7 virtual orb., 8 target st.
	8 virtual orb., 5 target st.
	9 virtual orb., 3 target st.

Table 2.5: MOLPRO calculated curves with their best R-matrix models

3. The cross sections calculations

The vibrational excitation (VE) cross sections were calculated using the local complex potential approximation implemented in program [15], based on numerical grid method introduced in [19, 20]. For LCP calculations the resonance width and energies are needed. These are also produced by the UKRmol suite of codes by fitting the eigenphase sums (1.21) with the Breit-Wigner formula (1.22). The typical energy dependence of the eigenphase sum for various internuclear distances is in Figure 3.1, for one fixed distance but different R-matrix models in Figure 3.2. The behaviour in both cases is expected: with growing internuclear distance the resonance energy and width decrease and by increasing the number of the virtual orbitals or target states more correlation gets considered and the resonce energy therefore decreases.

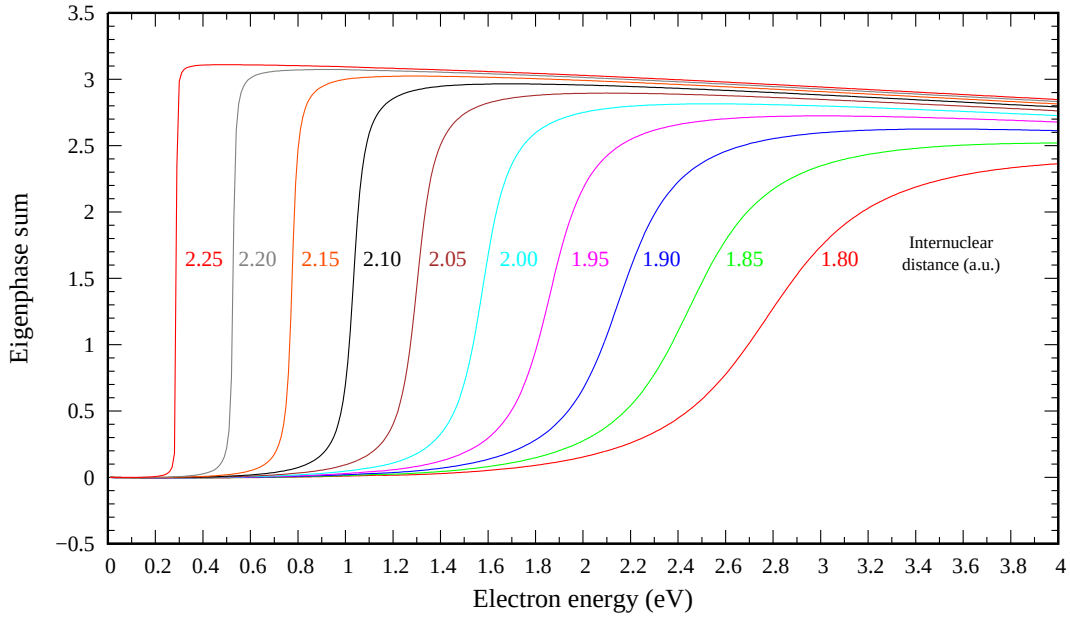

Figure 3.1: The energy dependence of the eigenphase sum with resonances for several internuclear distances for $9v, 3t$ R-matrix model.

3.1 Models comparison

The LCP calculations were performed for all models listed in Table 2.5 above. The vibrational excitation cross sections calculated for a specific Molpro curve with different R-matrix models can be seen in Figures 3.3, 3.4 and 3.5. The cross sections for all the curves with the common R-matrix model are in Figure 3.6.

From these figures one can see, that the position of a peak can move by up to 10 meV just by choosing the Molpro curve or changing the R-matrix model. A 10 meV shift is already comparable to the spin-orbital split magnitude. Another visible effect is the different spacing between individual peaks seen for different R-matrix models. This is visible for example for curve I for $8v, 5t$ and $9v, 4t$ R-matrix models. Their peaks are very close for lower energies, but with growing

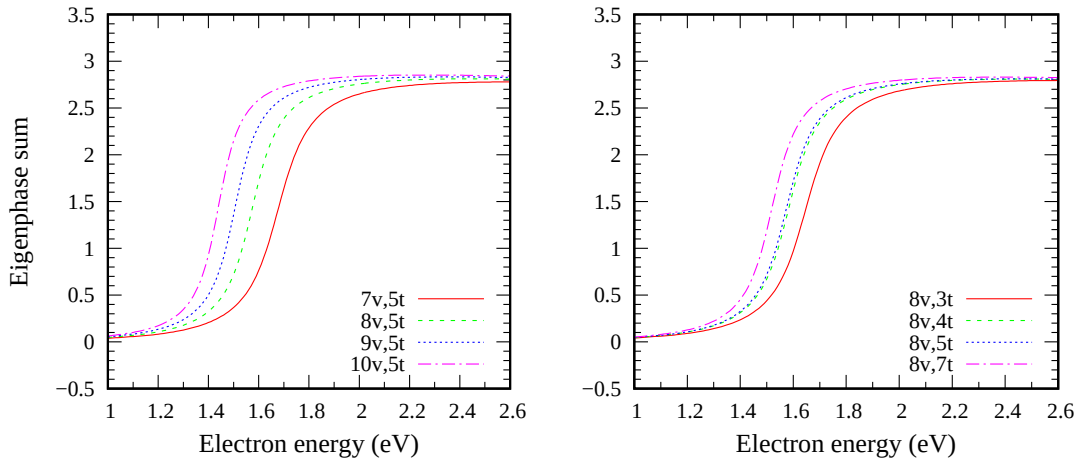

Figure 3.2: The energy dependence of the eigenphase sum for resonances for several different R-matrix models at a fixed internuclear distance 2 (a.u.).

energy they become distant. This plays an important role in choosing the final models in the next section.

3.2 Experiment comparison

As experimental data for comparison, measurements of Allan [21] were taken. Allan presents series of measurements of the cross sections for excitation of vibrational levels of $X^3\Sigma_g^-$ state of O_2 through $^2\Pi_g$ resonances.

The absolute heights of peaks measured by Allan come with quite a big uncertainty (about 35 %). Therefore Allan's cross sections are plotted in arbitrary units and scaled for a convenient comparison in all here presented graphs. Because of that, only the positions of peaks and their relative heights were considered relevant while comparing the results. Also the peak positions are accurate within ±30 meV range, which is larger than the spin-orbital splitting.

Furthermore the measurement is influenced by equipment's limited resolution, which was 10 meV for excitations $\nu = 1,\ 2,\ 3$, and 15 meV for the other. The resolution of the equipment was assumed to be Gaussian and all the calculated cross sections were convoluted

$$\sigma_\alpha(E) = \int_{E_{min}}^{E_{max}} \sigma(\varepsilon) g(\alpha, \varepsilon - E) \mathrm{d}\varepsilon, \tag{3.1}$$

where $\sigma(\varepsilon)$ is the calculated exact cross section, $\sigma_\alpha(E)$ the convoluted cross section to be compared to a measured one and $g(\alpha, \varepsilon - E)$ is the Gaussian distribution with α being the resolution (standard deviation)

$$g(\alpha, \varepsilon - E) = \frac{1}{\sqrt{2\pi}\alpha} \exp\left(-\frac{(\varepsilon - E)^2}{2\alpha^2}\right).$$

The importance of this step can be seen in Figure 3.7, which depicts the effect of convolution on the calculated cross section for $0 \to 1$ vibrational excitation,

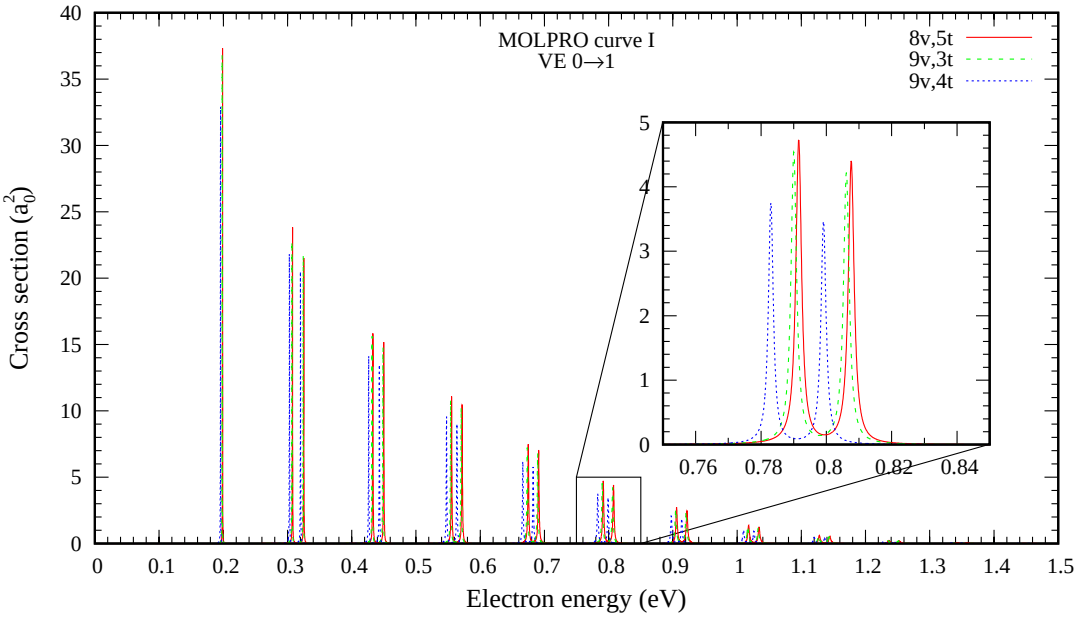

Figure 3.3: The LCP calculated cross section for VE $0 \rightarrow 1$ for MOLPRO curve I with several R-matrix models.

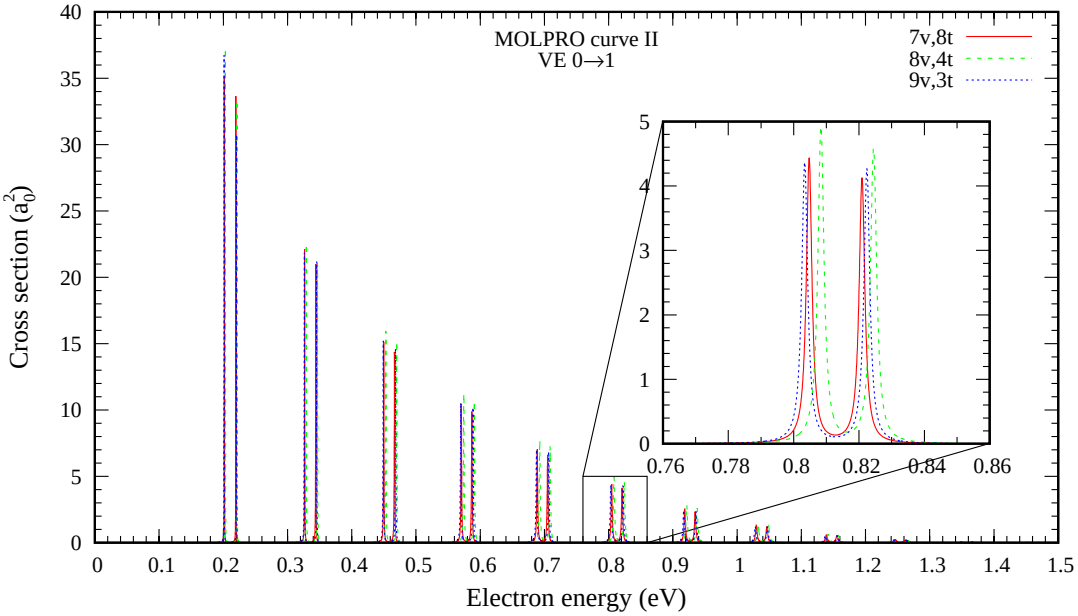

Figure 3.4: The same as in Figure 3.3, but for MOLPRO curve II.

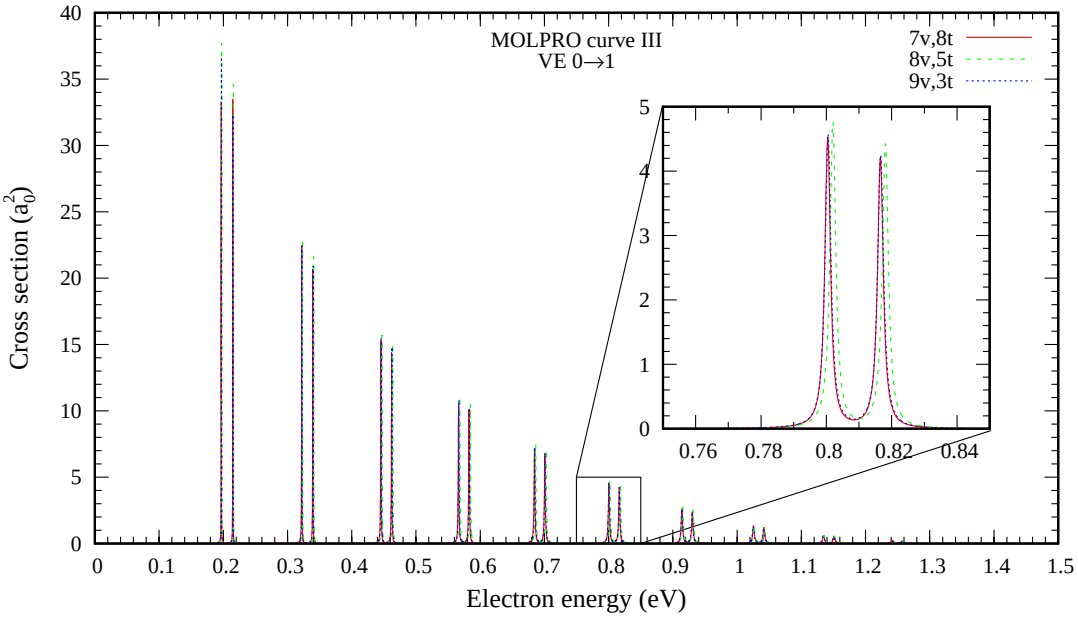

Figure 3.5: The same as in Figure 3.3, but for MOLPRO curve III.

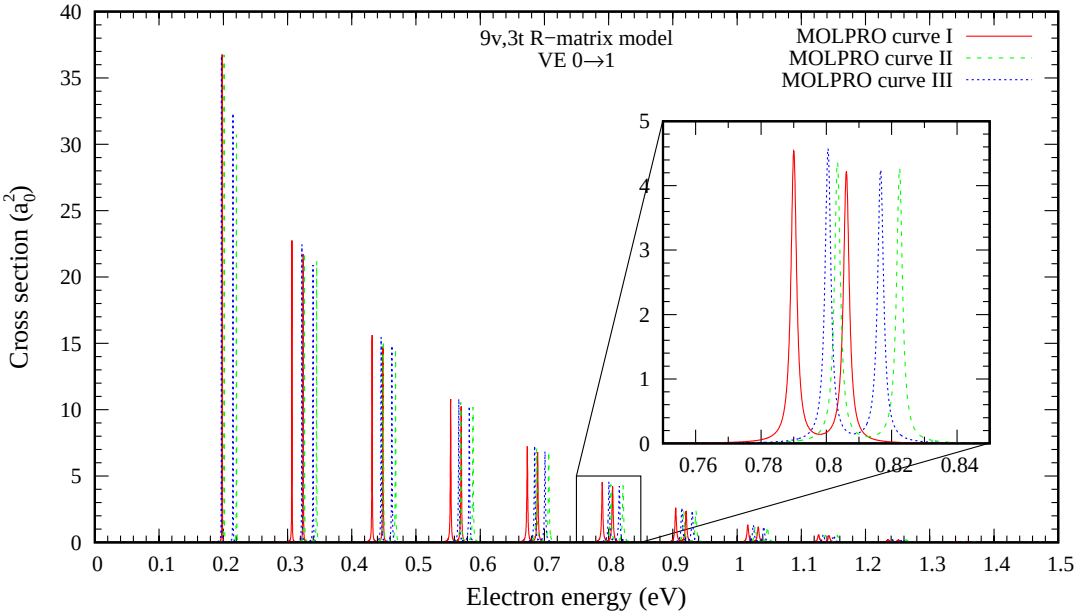

Figure 3.6: The LCP calculated cross section for VE $0 \rightarrow 1$ for the $9v, 3t$ R-matrix model with all considered MOLPRO curves.

compared to Allan's data. From now on, all presented data are convoluted with the finite resolution

The LCP calculations were performed for all the models listed in Table 2.5 for vibrational excitations $0 \to \nu$ for $\nu = 1 - 7$. Positions of peaks are compared in Figures 3.8, 3.9 and 3.10 to Allan's data only for VE $0 \to 1$, because these were presented in a graph with higher resolution than the other excitations.

For further evaluation a single model was chosen in two steps. First, the best model for each MOLPRO curve was selected, second, the best one of these three models was chosen. In the first step the folowing models seemed to be the most suitable:

curve I: 8 virtual orbitals, 5 target states,

curve II: 7 virtual orbitals, 8 target states,

curve III: 8 virtual orbitals, 5 target states.

These were chosen with respect to the uncertainty of experimental peak positions and are compared in Figure 3.11. The model with MOLPRO curve III, 8 virtual and 5 target states was the one with the most consistent peak spacing, in the second step.

For all channels, i.e. vibrational excitations $0 \to 1 \ldots 7$, the cross sections measured by Allan are depicted in Figure 3.12, the cross sections calculated with MOLPRO curve III and $8v, 5t$ R-matrix model are in Figure 3.13. In these figures, one important aspect is visible. Near the threshold energy of each channel there is a significant peak in the calculated cross sections, which is missing in Allan's measurements. The reason for this effect is probably the failure of the LCP approximation, which tends to produce very large cross sections just near the threshold energy, as demostrated for models of $e^- + N_2$ and $e^- + NO$ systems [22].

Allan integrated the cross sections through incident electron energy for each individual peak. As mentioned before, his data carry big uncertainty for peak heights and this uncertainty naturally persits through the integration. Relative areas of individual peaks with respect to the largest one are therefore taken for consideration. His results are in Table 3.1. The same was done with the cross sections calculated here. The positions of the peaks correspond to the energy gap between vibrational ground level of $X^3\Sigma_g^-$ state and the excited vibrational levels of $^2\Pi_g$. Midpoints of these positions were taken as integral interval bounds. Results for MOLPRO curve III and $8v, 5t$ R-matrix model are in Table 3.2. For the sake of readability the relative peak areas lower than 0.01 % were omitted in both tables.

While comparing the data one can see that the position of the highest peak agrees up to the vibrational level $\nu = 3$ of the $X^3\Sigma_g^-$ state. However the relative heights of the peaks agree poorly, again probably due to failure of the LCP approximation.

Better results could be obtained with different models of the nuclear dynamics, but that would reach beyond the extent of this work.

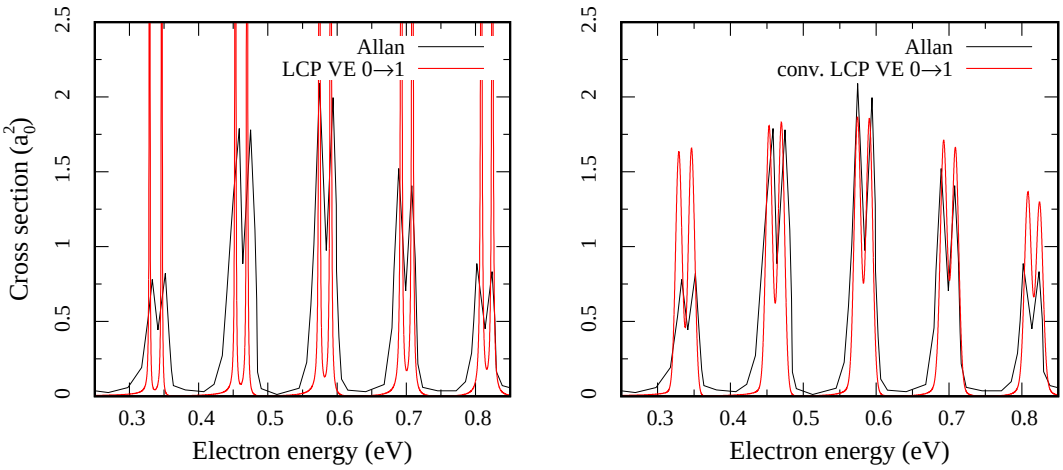

Figure 3.7: Comparison of the calculated VE $0 \rightarrow 1$ cross section (MOLPRO curve II, $8v, 4t$ R-matrix model) to the experimental result of Allan [21], left panel - without convolution, right panel - convoluted with 10 meV Gaussian

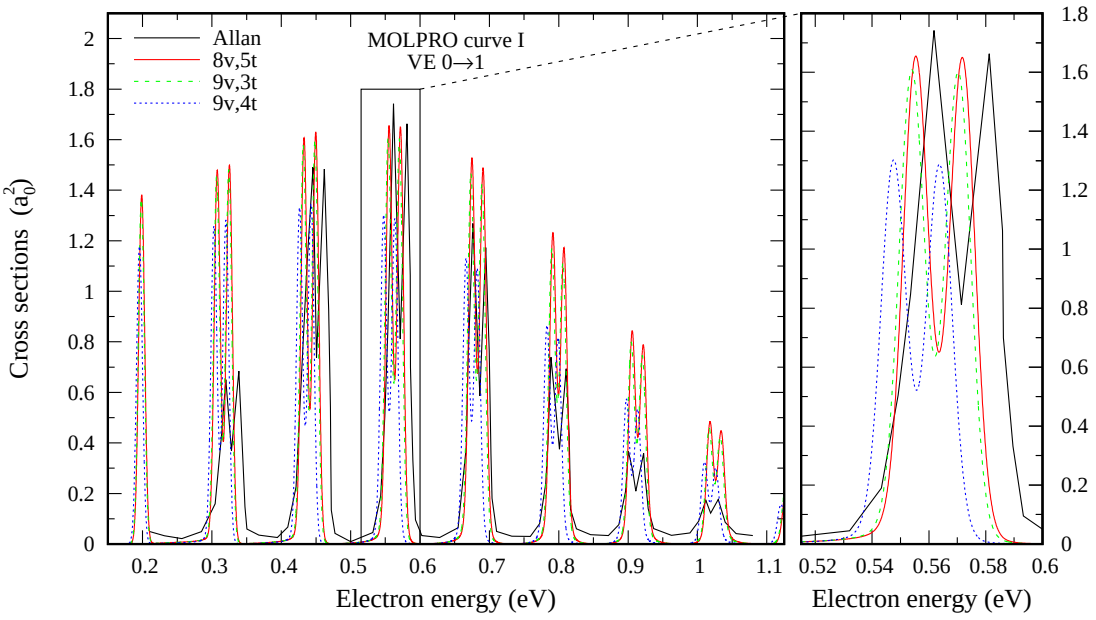

Figure 3.8: The cross section for VE $0 \rightarrow 1$, calculation results for MOLPRO curve I compared to the experimental data.

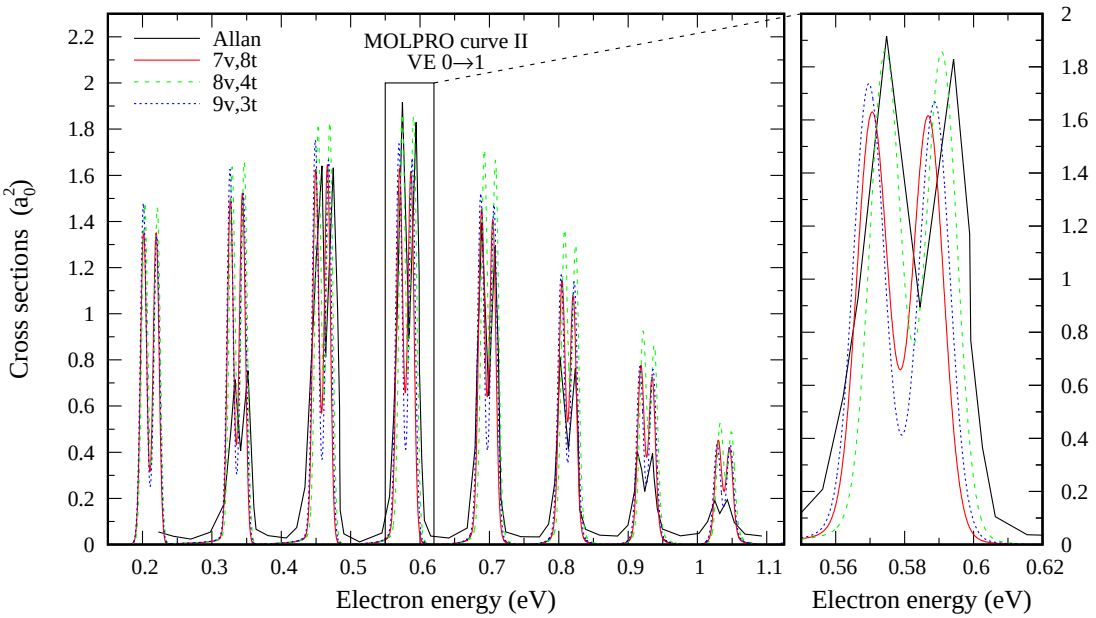

Figure 3.9: The same as in Figure 3.8, but for MOLPRO curve II.

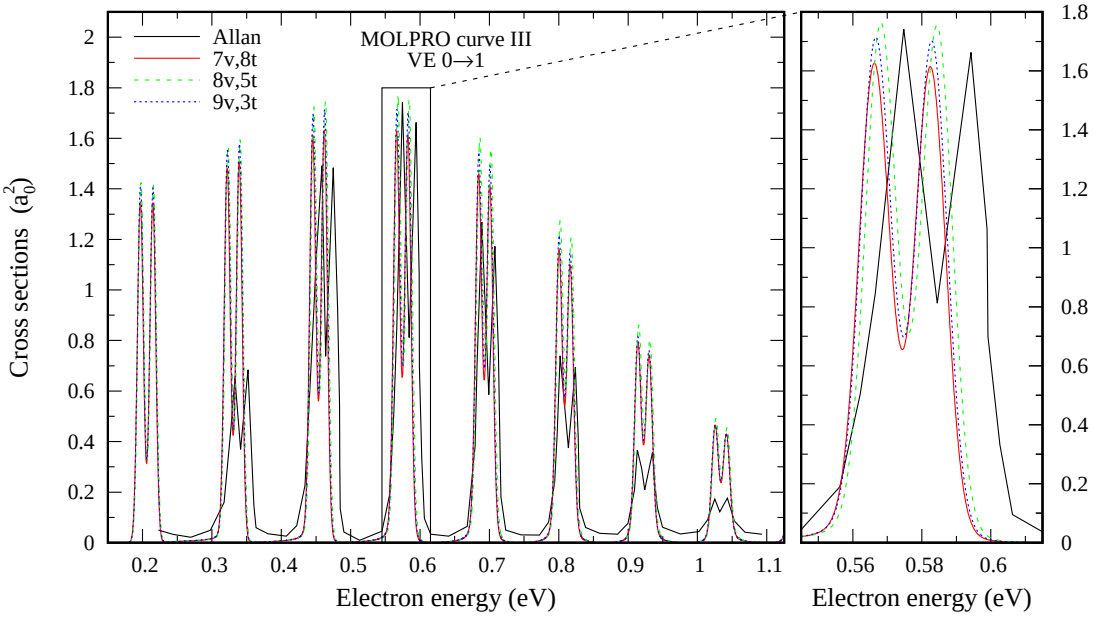

Figure 3.10: The same as in Figure 3.8, but for MOLPRO curve III.

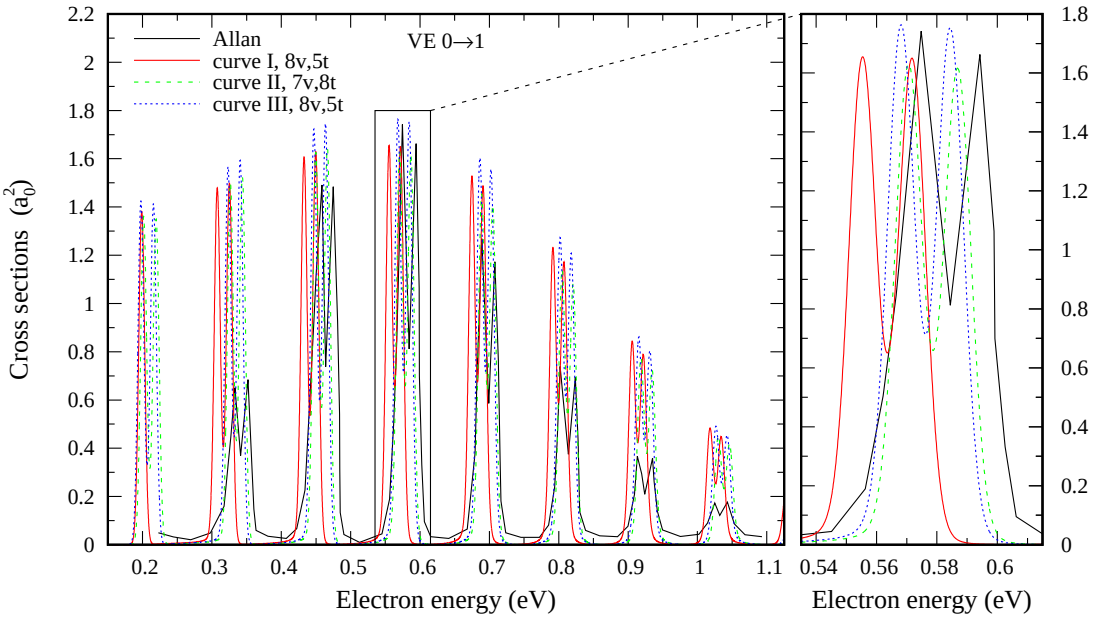

Figure 3.11: The cross section for vibrational excitation $0 \rightarrow 1$, the best three selected models compared to the experimental data.

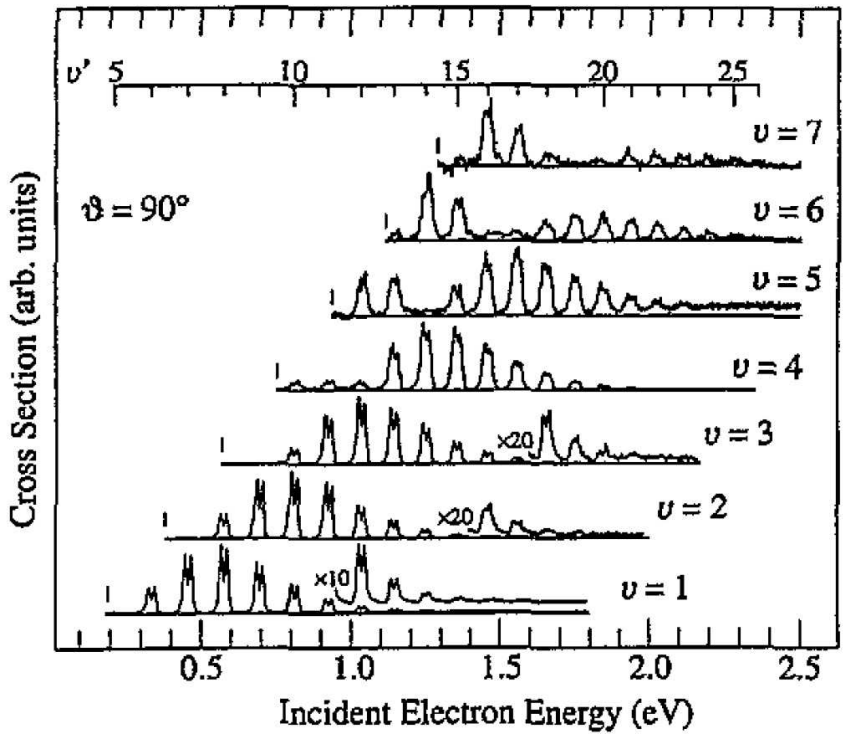

Figure 3.12: The experimental cross sections for vibrational excitation $0 \to 1 \ldots 7$, threshold energies are marked with vertical lines, © M. Allan, 1995 [21]

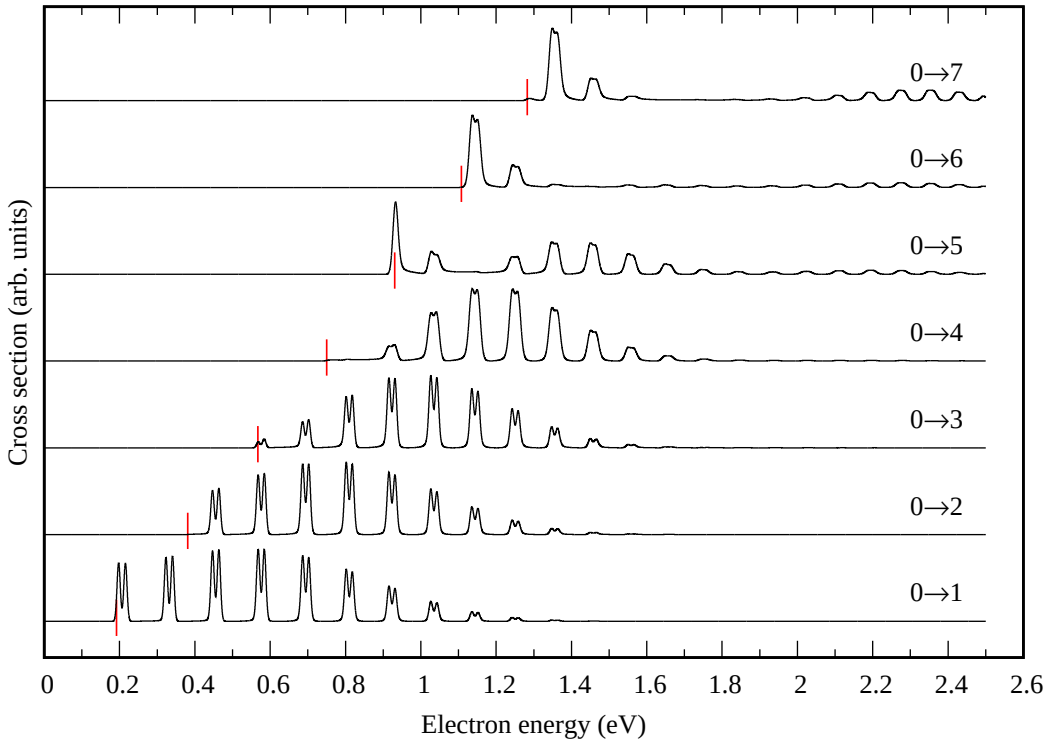

Figure 3.13: The LCP calculated cross sections for vibrational excitation $0 \to 1 \ldots 7$ for MOLPRO curve III with $8v, 5t$ R-matrix model; threshold energies are marked with vertical red lines.

	ν'									
	5	6	7	8	9	10	11	12	13	14
$\nu = 1$	0.009	0.458	0.979	1.000	0.713	0.413	0.201	0.090	0.042	0.019
$\nu = 2$	-	-	0.005	0.120	0.263	0.284	0.228	0.141	0.075	0.036
$\nu = 3$	-	-	-	-	-	0.017	0.048	0.063	0.054	0.036
$\nu = 4$	-	-	-	-	-	0.001	0.001	0.001	0.006	0.010
$\nu = 5$	-	-	-	-	-	-	-	0.001	0.001	-
$\nu = 6$	-	-	-	-	-	-	-	-	-	0.001
	15	16	17	18	19	20	21	22	23	24
$\nu = 1$	0.008	0.005	-	-	-	-	-	-	-	-
$\nu = 2$	0.017	0.007	0.003	0.002	-	-	-	-	-	-
$\nu = 3$	0.021	0.011	0.006	0.003	0.001	0.001	-	-	-	-
$\nu = 4$	0.009	0.007	0.004	0.003	0.001	0.001	-	-	-	-
$\nu = 5$	0.001	0.002	0.002	0.002	0.001	0.001	-	-	-	-
$\nu = 6$	-	-	-	-	-	-	-	-	-	-
$\nu = 7$	-	-	-	-	-	-	-	-	-	-

Table 3.1: Experimental areas [21] of resonance peaks in the cross sections for vibrational excitation of $X^3\Sigma_g^-$ state of O_2 to level ν via the ν' level of the $^2\Pi_g$ state of O_2^-, relative to the highest one - for $\nu = 1$ and $\nu' = 8$.

	ν'									
	5	6	7	8	9	10	11	12	13	14
$\nu = 1$:	0.752	0.865	0.964	1.000	0.922	0.744	0.514	0.301	0.150	0.064
$\nu = 2$:	-	-	0.327	0.444	0.530	0.549	0.483	0.358	0.224	0.119
$\nu = 3$:	-	-	-	0.018	0.071	0.135	0.184	0.191	0.158	0.106
$\nu = 4$:	-	-	-	-	-	0.002	0.011	0.030	0.043	0.042
$\nu = 5$:	-	-	-	-	-	-	0.006	0.004	0.001	0.003
$\nu = 6$:	-	-	-	-	-	-	-	-	0.011	0.003
	15	16	17	18	19	20	21	22	23	24
$\nu = 1$:	0.024	0.009	0.003	0.001	0.001	-	-	-	-	-
$\nu = 2$:	0.054	0.021	0.008	0.003	0.001	0.001	-	-	-	-
$\nu = 3$:	0.059	0.027	0.011	0.004	0.001	-	-	-	-	-
$\nu = 4$:	0.031	0.018	0.008	0.003	0.001	-	-	-	-	-
$\nu = 5$:	0.005	0.005	0.003	0.001	-	-	-	-	-	-
$\nu = 6$:	-	-	-	-	-	-	-	-	-	-
$\nu = 7$:	0.003	0.001	-	-	-	-	-	-	-	-

Table 3.2: Calculated areas of resonance peaks in the cross sections for vibrational excitation of $X^3\Sigma_g^-$ state of O_2 to level ν via the ν' level of the $^2\Pi_g$ state of O_2^- for curve III with $8v, 5t$ R-matrix model (the same as in Figure 3.13), relative to the highest one - for $\nu = 1$ and $\nu' = 8$.

Conclusion

In this work the resonant colisions of electrons with dioxygen were investigated. The potential energy curves of O_2 and O_2^- were obtained with standard quantum chemistry methods and the R-matrix method using several different models. The nuclear dynamics and the cross section for vibrational excitation were calculated within the local complex potential approximation and compared with experimental data.

We have shown that potential curves obtained in above described way can lead to the prediction of the resonance peaks within experimental uncertainty, however the local complex potential approximation seems to be insufficient, since it resulted in an unsatisfactory behaviour of the vibrational excitation cross sections, such as bad relative heights of individual peaks, especially near the channel threshold energies due to incorrect threshold behaviour of the LCP model.

In the future, different models of the nuclear dynamics will be tested, primarily the nonlocal resonance model [23] and its validity will be tested using a two-dimensional model presented in [22].

Bibliography

[1] Das, G., Wahl, A. C., Zemke, W.T. and Stwalley, W. C. *Accurate ab initio potential curves for the $X^2\Pi_g$, $A^2\Pi_u$, $a^4\Sigma_u^-$, and $^2\Sigma_u^-$ states of the O_2^- ion. J. Chem. Phys., 68 (1978) 4252.*

[2] Laporta, V., Celiberto and R., Tennyson, J. *Resonant vibrational-excitation cross sections and rate constants for low-energy electron scattering by molecular oxygen. Plasma Sources Sci. Technol., 20 (2013) 025001.*

[3] Ira N. Levine. *Quantum Chemistry.* Seventh edition. Pearson, New York, 2013.

[4] Z. Masin. *Resonance formation in electron collisions with pyrimidine-like targets.* PhD thesis, Department of Physical Sciences, The Open University, 2012.

[5] Friedrich, H. *Scattering Theory (Lecture Notes in Physics).* Springer, 2013.

[6] Dubé, L. and Herzenberg, A. *Absolute cross sections from the "boomerang model" for resonant electron-molecule scattering. Phys. Rev. A, 20 (1979) 194.*

[7] Werner, H.-J., Knowles, P. J., Knizia, G., Manby, F. R. and Schütz, M. *Molpro: a general purpose quantum chemistry program package. WIREs Comput Mol Sci, 2 (2012) 242.*

[8] Werner, H.-J., Knowles, P. J., Knizia, G., Manby, F. R. and Schütz, M. and others. *MOLPRO, version 2015.1, a package of ab initio programs*, 2015. see http://www.molpro.net.

[9] Werner, H.-J. and Knowles, P. J. *A Second Order MCSCF Method with Optimum Convergence. J. Chem. Phys., 82 (1985) 5053.*

[10] Knowles, P. J. and Werner, H.-J. *An Efficient Second Order MCSCF Method for Long Configuration Expansions. Chem. Phys. Let., 115 (1985) 259.*

[11] Knowles, P. J. and Werner, H.-J. *Internally Contracted Multiconfiguration Reference Configuration Interaction Calculations for Excited States. TCA, 84 (1992) 95.*

[12] Lide, D. *CRC handbook of chemistry and physics : a ready-reference book of chemical and physical data.* CRC Press, Boca Raton, Fla, 2009.

[13] Dunning, T. H. *Gaussian basis sets for use in correlated molecular calculations. I. The atoms boron through neon and hydrogen. J. Chem. Phys., 90 (1989) 1007.*

[14] Wilson, A. K., van Mourik, T. and Dunning, T. H. *Gaussian basis sets for use in correlated molecular calculations. VI. Sextuple zeta correlation consistent basis sets for boron through neon. J. Mol. Struct., 388 (1996) 339.*

[15] Houfek, K. LCP approximation for diatomic molecules, 2010. see http://utf.mff.cuni.cz/Quantum/software/lcp.htm.

[16] Helgaker, T., Jørgensen, P. and Olsen, J. *Molecular electronic-structure theory*. Wiley, 2000.

[17] Werner, H.-J. and Knowles, P. J. *MOLPRO User's Guide 2012.1*. University College Cardiff Consultants Limited.

[18] Carr, J. M., Galiatsatos, P. G., Gorfinkiel, J. D., Harvey, A. G., Lysaght, M. A., Madden, D., Masin, Z., Plummer, M., Tennyson, J. and Varambhia, H. N. *UKRmol: A low-energy electron- and positron-molecule scattering suite. EPJ D, 66 (2012).*

[19] Rescigno, T. N., McCurdy, C. W. *Numerical grid methods for quantum-mechanical scattering problems. Phys. Rev. A, 62 (2000) 032706.*

[20] McCurdy, C. W., Baertschy, M., Rescigno, T. N. *Solving the three-body Coulomb breakup problem using exterior complex scaling. J. Phys. B, 37 (2004) R137-R187.*

[21] Allan, M. *Measurement of absolute differential cross sections for vibrational excitation of O_2 by electron impact. J. Phys. B, 28 (1995) 5163.*

[22] Houfek, K., Rescigno, T. N., McCurdy, C. W. *Numerically solvable model for resonant collisions of electrons with diatomic molecules. Phys. Rev. A, 73 (2006) 032721.*

[23] Domcke, W. *Theory of resonance and threshold effects in electron molecule collisions - the projection-operator approach. Phys. Rep., 208 (1991) 97.*